AIAA JOURNAL
Vol. 46, No. 7, July 2008

Interpolation Method for Adapting Reduced-Order Models and Application to Aeroelasticity

David Amsallem* and Charbel Farhat†
Stanford University, Stanford, California 94305-3035

DOI: 10.2514/1.35374

Reduced-order models are usually thought of as computationally inexpensive mathematical representations that offer the potential for near real-time analysis. Although most reduced-order models can operate in near real-time, their construction can be computationally expensive, as it requires accumulating a large number of system responses to input excitations. Furthermore, reduced-order models usually lack robustness with respect to parameter changes and therefore must often be rebuilt for each parameter variation. Together, these two issues underline the need for a fast and robust method for adapting precomputed reduced-order models to new sets of physical or modeling parameters. To this effect, this paper presents an interpolation method based on the Grassmann manifold and its tangent space at a point that is applicable to structural, aerodynamic, aeroelastic, and many other reduced-order models based on projection schemes. This method is illustrated here with the adaptation of computational-fluid-dynamics-based aeroelastic reduced-order models of complete fighter configurations to new values of the freestream Mach number. Good correlations with results obtained from direct reduced-order model reconstruction, high-fidelity nonlinear and linear simulations are reported, thereby highlighting the potential of the proposed reduced-order model adaptation method for near real-time aeroelastic predictions using precomputed reduced-order model databases.

Nomenclature

$\bar{\mathbf{B}}$	=	aeroelastic coupling matrix
$\bar{\mathbf{B}}_r$	=	nondimensional reduced-order aeroelastic coupling matrix
Exp_S	=	exponential operator at the point $\mathcal{S}$
$\mathbf{f}^{\mathrm{ext}}$	=	vector of external forces applied to the structural subsystem
$\mathcal{G}(,)$	=	Grassmann manifold
$\bar{\mathbf{H}}$	=	first-order term of the Taylor expansion of the nondimensional numerical fluid flux function
$\bar{\mathbf{H}}_r$	=	nondimensional reduced-order fluid subsystem matrix
$\mathbf{I}_n$	=	identity matrix of size n
$\log_S$	=	logarithmic operator at the point $\mathcal{S}$
$\mathcal{M}$	=	set of freestream Mach numbers
M_∞	=	freestream Mach number
N_Φ	=	size of the reduced-order basis
N_f	=	dimension of the full-order model
N_m	=	number of natural modes of the dry structure
N_p	=	number of parameters per operating point
N_R	=	number of precomputed reduced-order models
N_s	=	dimension of the structural model
$\mathbf{P}$	=	linearization of the external load with respect to the nondimensional fluid state vector
$\mathbb{R}$	=	real axis
$\tilde{r}$	=	reduced interpolation parameter
$\mathcal{ST}(,)$	=	Stiefel manifold
$\mathcal{S}$	=	subspace of $\mathbb{R}^{N_f}$ of dimension N_Φ
s	=	physical or modeling parameter
T	=	transpose operation
$\mathcal{T}_\mathcal{S}$	=	tangent space to a Grassmann manifold at the point $\mathcal{S}$
$\mathbf{U}$	=	matrix of left singular orthonormal basis vectors associated with a thin singular value decomposition
$\bar{\mathbf{u}}$	=	nondimensional vector of structural displacements
$\mathbf{u}_m$	=	generalized (modal) displacement coordinates of the structure
$\mathbf{V}$	=	matrix of right singular orthonormal basis vectors associated with a thin singular value decomposition
$\bar{\mathbf{w}}$	=	nondimensional conservative state vector of the fluid subsystem
$\bar{\mathbf{w}}_r$	=	projection of the nondimensional full-order fluid state vector on the proper orthogonal decomposition basis
$\mathbf{X}$	=	matrix of mode shapes of the dry structure
$\mathcal{Y}(t)$	=	geodesic path on a manifold
$\mathcal{Y}_0$	=	initial point for a geodesic path on a manifold
$\dot{\mathcal{Y}}_0$	=	initial derivative for a geodesic path on a manifold
$\bar{\mathbf{y}}$	=	vector of structural displacements and velocities in state-space form
α	=	angle of attack
Γ	=	matrix representing the coordinates of a point of a tangent space to a Grassmann manifold
Λ	=	set of operating points
λ	=	operating point
$\mathbf{\Sigma}$	=	matrix of singular values
$,\tau$	=	partial derivative with respect to nondimensional time τ
$\mathbf{\Phi}, \mathbf{\Psi}$	=	reduced-order orthogonal basis vectors
χ	=	point on a tangent space to a Grassmann manifold
$\mathbf{\Omega}$	=	diagonal matrix of the natural pulsations of the structural subsystem
$\dot{()}$	=	partial derivative with respect to time

Received 29 October 2007; revision received 27 February 2008; accepted for publication 13 March 2008.

*Graduate Student, Department of Aeronautics and Astronautics, Building 500, 488 Escondido Mall. AIAA Member.

†Professor, Department of Mechanical Engineering, Institute for Computational and Mathematical Engineering, and Department of Aeronautics and Astronautics (by courtesy), Building 500, 488 Escondido Mall. AIAA Fellow.

I. Introduction

DURING the last two decades, giant strides have been achieved in many aspects of computational engineering and sciences. Higher-order mathematical models, better approximation methods, and faster solution algorithms have been developed for many engineering applications. Computing speed barriers have also been shattered by hardware manufacturers. As a result, high-fidelity, physics-based mathematical models have become central to advances in almost all areas of engineering and science. These

models emphasize, as much as possible, detailed representations to "avoid missing something." For many applications, however, they remain computationally intensive and therefore are more often used in special circumstances rather than routinely. This is the case for nonlinear aeroelastic simulations based on computational fluid dynamics (CFD). Indeed, nonlinear, CFD-based aeroelastic models typically entail a major computational cost, which is incurred by the need for high-fidelity fluid models to resolve the complex flow patterns present, for example, in the transonic regime. This cost is such that CFD-based nonlinear aeroelastic codes are applied nowadays to the analysis of a few, carefully chosen, configurations, rather than routine analysis.

The last decade has also been marked by advances in the construction of reduced-order models (ROMs) using a variety of projection methods. Unlike high-fidelity models, these seek the simplest mathematical representation that captures the dominant behavior of the system to be simulated. They are usually low-dimensional in the sense that they involve a much smaller number of degrees of freedom (DOF) or unknowns than their high-fidelity counterparts. As such, they can operate in near real time. For this reason, and because they can be sufficiently accurate, ROMs are often sought after for many applications pertaining to design [1], design optimization [2], control [3], and dynamic data-driven systems [4,5], among others.

In the field of aeronautics, many approaches for constructing linear fluid and aeroelastic ROMs have been developed and shown to produce numerical results that compare well with those generated by high-fidelity, nonlinear counterparts [6–19]. Among these approaches, the proper orthogonal decomposition (POD) method [20,21] is perhaps the most popular. For example, the POD was successfully applied to the CFD-based aeroelastic analysis of a transport aircraft model [22] and two complete fighter jet configurations [23–28].

Unfortunately, design optimization, control, data-driven systems, and many other applications typically involve parameter changes, and most, if not all, linear ROM technologies lack robustness with respect to parameter variations. For example, a POD-based fluid ROM is very sensitive to the freestream Mach number. In particular, it does not approximate well the dynamics of the fluid flow when the freestream Mach number is different from that used for constructing the underlying POD basis, as shown in Sec. V.C of this paper. Therefore, performing "dynamic" computations using ROMs calls for constructing a new ROM each time a sensitive physical or modeling parameter is varied. However, reconstructing a ROM is, in many cases, a computationally intensive proposition, as it requires accumulating new system responses from a new set of high-fidelity numerical simulations. For example, it was shown in [25] that for a complete F-16 configuration at $M_\infty = 0.9$, the construction by the POD method of a CFD-based aeroelastic ROM with 69 DOF requires 3.85 h CPU time on a 15-processor Linux cluster. Of this CPU time, 95% is consumed by the calculation in the frequency domain of 99 snapshots associated with a high-fidelity aeroelastic model composed of a finite element (FE) representation of the structure with 168,799 DOF and a CFD representation of the inviscid flow with 2.019595×10^6 conservative variables. In comparison, predicting a few cycles of the aeroelastic response of the F-16 aircraft using the constructed ROM requires on the order of 1 min CPU time on a single processor of the same Linux cluster. This example highlights the difference between the CPU time associated with exploiting a ROM and that required for constructing it. It also underscores the need for a fast computational algorithm for adapting a precomputed ROM (or set of ROMs) to changes in the physical or modeling parameters.

To address the aforementioned ROM adaptation issue, at least three approaches have been considered in the aeronautical literature in the context of the POD method: the global POD (GPOD) [29–31], the method of direct interpolation of the reduced-order basis vectors [15], and the subspace angle interpolation method [15,23,24,26].

The basic idea behind the GPOD approach is to enrich the snapshot matrix with solutions corresponding to different values of the varied parameter(s). Not only does this approach naturally lose the optimal approximation property of the POD method, but, in many cases, it is not reliable. For example, it fails to properly adapt an aeroelastic ROM in the transonic regime to variations in the freestream Mach number or angle of attack [25].

As its name suggests, the direct interpolation approach constructs a new reduced-order basis associated with a new set of physical or modeling parameters by interpolating reduced-order bases that were precomputed for previous values of these parameters. Unfortunately, this simple approach is also doomed to failure. For example, in the case of the POD method, the reduced-order basis vectors are orthogonal but the interpolation of orthogonal vectors is not guaranteed to construct a new set of orthogonal vectors. Furthermore, this approach was also shown to fail for aeroelastic applications in the transonic regime [15,32].

The subspace angle interpolation approach adapts two ROMs associated with two different values of the physical or modeling parameter to a new parameter value by linearly interpolating the subspace angles between the two precomputed reduced-order bases, rather than directly interpolating the vectors of these reduced-order bases. This approach, which was introduced in [15], was successfully demonstrated in the context of the POD method and aeroelastic analysis of full aircraft configurations, when the freestream Mach number or angle of attack is varied [23–26]. However, the subspace angle interpolation approach is a low-order interpolation method. Therefore, as shown in [24,26], this is either inaccurate when the two parameters are far apart, or computationally inefficient when restricted to the interpolation between two precomputed reduced-order bases corresponding to two parameters that are sufficiently close.

In this paper, an alternative method is proposed for adapting precomputed ROMs to changes in physical or modeling parameters. This method, which is applicable to any set of ROMs for which a corresponding set of reduced-order bases can be identified, is based on notions and results from differential geometry. These include the Grassmann manifold, its tangent space at a point, and the computation of geodesic paths on this manifold. The proposed ROM adaptation method also involves interpolation. However, it recognizes the fact that the interpolation problem typically involves some constraints; for example, an orthogonality property of the reduced-order basis as in the case of the POD or modal reduction method. For this reason, the proposed adaptation method first transports the precomputed reduced-order bases to a "flat," constraint-free space. Next, it interpolates in this space the parametric data using a conventional approximation method. Finally, it transports back the interpolated result to the originating space, where it constructs the sought-after reduced-order basis and adapted ROM. Furthermore, the new ROM adaptation method is shown to posses a relatively low computational complexity and to be robust. As such, it paves the way for near real-time prediction strategies based on ROM databases, ROM adaptation, and ROM processing.

The remainder of this paper is organized as follows. First, the adaptation problem of interest is formulated in Sec. II. Then, relevant notions and results from differential geometry are reviewed in Sec. III. Next, a computational framework for ROM adaptation based on interpolation in a vector space is proposed in Sec. IV. In particular, it is shown that this framework includes as a particular case the low-order subspace angle interpolation method [15,23,24,26]. The proposed method is applied in Sec. V to the adaptation of aeroelastic ROMs of F-16 and F/A-18 fighter aircraft to new freestream Mach numbers. Finally, conclusions are offered in Sec. VI.

II. Problem Formulation

Consider the case of ROMs based on reduced-order bases such as those constructed by the POD method or some form of modal reduction method. Usually, such bases are constructed for given sets of physical and/or modeling parameters, each of which is referred to in this paper as an "operating point." An important and practical issue associated with such bases and their corresponding ROMs is their lack of robustness with respect to parameter changes. Interpolation is

a natural and attractive idea for adapting them to a new operating point. Unfortunately, it is not a straightforward task. For example, reduced-order bases constructed using the POD and modal analysis methods are orthogonal, but the standard interpolation of orthogonal vectors does not necessarily produce a set of orthogonal vectors. More generally, the standard interpolation of a set of bases does not necessarily produce a basis. For this reason, a more appropriate adaptation method, which nevertheless involves an interpolation component, is sought after in this paper. To this effect, the ROM adaptation problem is formulated here as follows.

Problem. Let $N_R > 1$ ROMs of the same dimension and their corresponding orthogonal reduced-order bases constructed at N_R operating points λ_j, with $\lambda_j \neq \lambda_i$ for $j \neq i$, be given, and let Λ denote the set of respective operating points of these ROMs:

$$\Lambda = \{\lambda_0, \lambda_1, \ldots, \lambda_{N_R-1}\} \tag{1}$$

Interpolate the given reduced-order bases to rapidly construct a new ROM that can reliably operate at $\lambda_{N_R} \notin \Lambda$.

III. Review of Some Notions and Results from Differential Geometry

A. Grassmann Manifold and Its Tangent Space at a Point

Let $\mathbf{\Phi}_0 \in \mathbb{R}^{N_f \times N_\Phi}$, where $N_\Phi \leq N_f$, denote the full-rank column matrix associated with a ROM. The columns of $\mathbf{\Phi}_0$ provide a basis of the subspace $\mathcal{S}_0$ of dimension N_Φ in $\mathbb{R}^{N_f}$. This subspace $\mathcal{S}_0$ belongs to the Grassmann manifold [33–37] $\mathcal{G}(N_\Phi, N_f)$, which is defined as the set of all N_Φ-dimensional subspaces of $\mathbb{R}^{N_f}$. More generally, each N_Φ-dimensional subspace $\mathcal{S}$ of $\mathbb{R}^{N_f}$ can be viewed as a point of $\mathcal{G}(N_\Phi, N_f)$ and nonuniquely represented by a matrix $\mathbf{\Phi} \in \mathbb{R}^{N_f \times N_\Phi}$ whose columns span the subspace $\mathcal{S}$.[‡] For these reasons, the Grassmann manifold offers a suitable framework for manipulating reduced-order bases. The matrices $\mathbf{\Phi}$ belong to the so-called noncompact Stiefel manifold $\mathcal{ST}(N_\Phi, N_f)$ [33,37], which is defined as the set of all $N_f \times N_\Phi$ matrices of rank N_Φ. In this work, the matrices $\mathbf{\Phi}$ are chosen among those whose columns form a set of orthonormal vectors of $\mathbb{R}^{N_f}$. Therefore, they are chosen in the compact Stiefel manifold [33] which is the subset of orthonormal matrices in $\mathcal{ST}(N_\Phi, N_f)$. There exists a projection map [33] from $\mathcal{ST}(N_\Phi, N_f)$ to $\mathcal{G}(N_\Phi, N_f)$, as each matrix $\mathbf{\Phi}$ in $\mathcal{ST}(N_\Phi, N_f)$ spans a subspace of $\mathbb{R}^{N_f}$ of dimension N_Φ and different matrices can span the same subspace. At each point $\mathcal{S}$ of the manifold $\mathcal{G}(N_\Phi, N_f)$, there exists a tangent space [33,37] of the same dimension [37]. This space is denoted by $\mathcal{T}_\mathcal{S}$ and each of its points can be represented by a matrix $\Gamma \in \mathbb{R}^{N_f \times N_\Phi}$. This tangent space is a vector space which has its origin at the point of tangency. Hence, $\mathcal{T}_\mathcal{S}$ is a flat space: that is, a space in which interpolation can be performed as usual.

B. Geodesic Path on a Grassmann Manifold

A geodesic is defined as the shortest path [40] between two points of a differential manifold. For example, a geodesic on a sphere is a great circle. This path is also a trajectory associated with a second-order ordinary differential equation [34,37,41]. Thus, a geodesic path is uniquely defined by two initial conditions. These are typically its initial position and initial derivative [40]. A geodesic path can be parameterized by a scalar variable, denoted here by t, so that it can be represented by a twice differentiable function $\mathcal{Y}(t), 0 \leq t \leq 1$. In this case, $\mathcal{Y}(0)$ is the initial point of the geodesic and $\mathcal{Y}(1)$ is its final point. As the initial derivative $\dot{\mathcal{Y}}(0)$ belongs to the tangent space at $\mathcal{Y}(0)$, there is a fundamental link between the concept of a geodesic and that of the exponential mapping which maps a tangent space to the manifold itself [33,34,40,41]. This link is established by the following mathematical result.

[‡]The Grassmann manifold $\mathcal{G}(N_\Phi, N_f)$ is rigorously of dimension $N_\Phi \times (N_f - N_\Phi)$. However, in the present work, a matrix with columns spanning the subspace of size $N_f \times N_\Phi$ is preferred to canonical coordinates such as the Plucker–Grassmann [38] coordinates to represent a point of this manifold. This is a common approach [37,39] as the Plucker–Grassmann coordinates are not practical from the computational viewpoint.

Result 1. Let $\mathcal{Y}(t)$ be the geodesic path on a manifold $\mathcal{M}$ such as $\mathcal{G}(N_\Phi, N_f)$ that is uniquely determined by the initial conditions $(\mathcal{Y}(0), \dot{\mathcal{Y}}(0)) = (\mathcal{Y}_0, \dot{\mathcal{Y}}_0)$. Then, the exponential of $\dot{\mathcal{Y}}_0$, denoted by $\mathrm{Exp}_{\mathcal{Y}_0}(\dot{\mathcal{Y}}_0)$, is given by

$$\mathrm{Exp}_{\mathcal{Y}_0}(\dot{\mathcal{Y}}_0) = \mathcal{Y}(1) \tag{2}$$

In the case of a Grassmann manifold, an explicit formula for the exponential mapping between a point of a tangent space to the manifold and the manifold itself is given by the following additional result [39].

Result 2. Let $\mathbf{\Psi}$ denote an orthogonal matrix whose columns span $\mathcal{S} \in \mathcal{G}(N_\Phi, N_f)$ and χ denote a point of $\mathcal{T}_\mathcal{S}$ spanned by the columns of a matrix Γ. The exponential mapping $\mathrm{Exp}_\mathcal{S}$ maps χ to an N_Φ-dimensional subspace $\mathcal{S}'$ represented by an orthogonal matrix $\mathbf{\Psi}' \in \mathbb{R}^{N_f \times N_\Phi}$, and based on the thin singular value decomposition (SVD) [39]

$$\Gamma = \mathbf{U}\mathbf{\Sigma}\mathbf{V}^T \qquad \text{(thin SVD)} \tag{3}$$

$$\mathbf{\Psi}' = \mathbf{\Psi}\mathbf{V}\cos(\mathbf{\Sigma}) + \mathbf{U}\sin(\mathbf{\Sigma}) \tag{4}$$

In Eq. (3), $\mathbf{\Sigma} \in \mathbb{R}^{N_\Phi \times N_\Phi}$ is a diagonal matrix containing the singular values of Γ and $\mathbf{U} \in \mathbb{R}^{N_f \times N_\Phi}$ and $\mathbf{V} \in \mathbb{R}^{N_\Phi \times N_\Phi}$ are orthogonal matrices.

The inverse of the exponential map, known as the logarithmic map, is denoted by $\log_\mathcal{S}$ and defined in a neighborhood [36,40] of $\mathcal{S} \in \mathcal{G}(N_\Phi, N_f)$. Given an origin point of the manifold, it defines a mapping between a neighborhood of this point and the tangent space to the manifold at that origin. The following result enables the practical computation of the logarithmic map.

Result 3. Let $\mathbf{\Psi}$ and $\mathbf{\Psi}'$ denote two orthogonal matrices whose columns span a subspace $\mathcal{S}$ and a subspace $\mathcal{S}'$ in the neighborhood of $\mathcal{S}$, respectively. The image of $\mathcal{S}'$ by the logarithmic map $\log_\mathcal{S}$, $\chi = \log_\mathcal{S}\mathcal{S}' \in \mathcal{T}_\mathcal{S}$, is represented by the matrix Γ given by [39]

$$(\mathbf{I} - \mathbf{\Psi}\mathbf{\Psi}^T)\mathbf{\Psi}'(\mathbf{\Psi}^T\mathbf{\Psi}')^{-1} = \mathbf{U}\mathbf{\Sigma}\mathbf{V}^T \qquad \text{(thin SVD)} \tag{5}$$

$$\Gamma = \mathbf{U}\tan^{-1}(\mathbf{\Sigma})\mathbf{V}^T \tag{6}$$

Note that $\log_\mathcal{S}\mathcal{S} = 0_{N_f \times N_\Phi}$, which makes the point $\mathcal{S}$ the origin of the tangent space at $\mathcal{S}$.

An explicit parameterization of the geodesic path is given by the following fourth mathematical result [33].

Result 4. Let $\mathbf{\Psi}$ be an orthogonal matrix representing $\mathcal{Y}_0 \in \mathcal{G}(N_\Phi, N_f)$ and

$$\Gamma = \mathbf{U}\mathbf{\Sigma}\mathbf{V}^T \qquad \text{(thin SVD)} \tag{7}$$

be the matrix representing $\chi \in \mathcal{T}_{\mathcal{Y}_0}$. The parametric representation of the geodesic path on $\mathcal{G}(N_\Phi, N_f)$ with initial conditions $(\mathcal{Y}(0) = \mathcal{Y}_0, \dot{\mathcal{Y}}(0) = \chi)$ is given by [33,37]

$$\mathcal{Y}(t) = \mathrm{span}[\mathbf{\Psi}\mathbf{V}\cos(t\mathbf{\Sigma}) + \mathbf{U}\sin(t\mathbf{\Sigma})] \qquad 0 \leq t \leq 1 \tag{8}$$

Note that Eqs. (4) and (8) are compatible with the general definition of the exponential map given in Eq. (2).

IV. Computational Framework for ROM Adaptation Based on Interpolation in Vector Space

Given 1) a set of N_R precomputed reduced-order bases characterized by the same dimension N_Φ but different operating points

$$\{\lambda_i\}_{i=0}^{N_R-1}$$

2) their corresponding matrices

$$\{\mathbf{\Psi}_i \in \mathbb{R}^{N_f \times N_\Phi}\}_{i=0}^{N_R-1}$$

and 3) the basic data needed for constructing a ROM from a given reduced-order basis (usually, a high-fidelity model), the ROM adaptation method proposed in this paper first constructs a new reduced-order basis for a new operating point $\lambda_{N_R} \notin \Lambda$ [see Eq. (1)] and the corresponding matrix $\mathbf{\Psi}_{N_R} \in \mathbb{R}^{N_f \times N_\Phi}$, then constructs the sought-after adapted ROM from the knowledge of the basic data and $\mathbf{\Psi}_{N_R}$: for example, by projecting these data onto $\mathbf{\Psi}_{N_R}$. In this section, this ROM adaptation method is first described in the particular case of two precomputed reduced-order bases ($N_R = 2$) and a single physical or modeling parameter per operating point. Next, it is formalized for the general case of an arbitrary number of precomputed reduced-order bases N_R and an arbitrary number of parameters per operating point N_p. The discussion of the aforementioned special case is not necessary for specifying the proposed ROM adaptation method. However, it highlights its differential geometry interpretation, which is expected to ease the understanding of this method by the reader. Finally, it is mentioned that it was recently proved that the subspace angle interpolation method [15,23,24,26] is a particular, low-order case, of the proposed ROM adaptation method.

A. Special Case of Two Precomputed Bases and One Parameter per Operating Point

Let $\mathbf{\Psi}_0 \in \mathbb{R}^{N_f \times N_\Phi}$ and $\mathbf{\Psi}_1 \in \mathbb{R}^{N_f \times N_\Phi}$ represent two reduced-order bases precomputed at two different operating points λ_0 and λ_1, corresponding to two different values s_0 and s_1 of a physical or modeling parameter s. The proposed procedure for adapting the two available reduced-order bases to a new operating point $\tilde{\lambda}$ corresponding to a value $\tilde{s}$ of s that is different from both s_0 and s_1 can be described in this case as follows.

Let $\mathcal{S}_0$ and $\mathcal{S}_1$ denote the two points of $\mathcal{G}(N_\Phi, N_f)$ that are spanned by the columns of the matrices $\mathbf{\Psi}_0$ and $\mathbf{\Psi}_1$, respectively, and let $\mathcal{Y}(t)$ denote the geodesic between these two points with $\mathcal{S}_0$ chosen as its origin; that is, the geodesic on $\mathcal{G}(N_\Phi, N_f)$ satisfying $\mathcal{Y}(0) = \mathcal{S}_0$ and $\mathcal{Y}(1) = \mathcal{S}_1$.

Let $\mathcal{T}_{\mathcal{S}_0}$ denote the tangent space to $\mathcal{G}(N_\Phi, N_f)$ at $\mathcal{S}_0$ containing the initial derivative $\dot{\mathcal{Y}}(0)$. From Eq. (2) of Result 1, it follows that

$$\dot{\mathcal{Y}}_0 = \dot{\mathcal{Y}}(0) = \log_{\mathcal{S}_0}(\mathcal{S}_1) \tag{9}$$

and from Eqs. (5) and (6) of Result 3, it follows that the matrix representing the initial derivative $\dot{\mathcal{Y}}_0$ is given by

$$\left(\mathbf{I} - \mathbf{\Psi}_0\mathbf{\Psi}_0^T\right)\mathbf{\Psi}_1\left(\mathbf{\Psi}_0^T\mathbf{\Psi}_1\right)^{-1} = \mathbf{U}\mathbf{\Sigma}\mathbf{V}^T \qquad \text{(thin SVD)} \tag{10}$$

$$\Gamma = \mathbf{U}\tan^{-1}(\mathbf{\Sigma})\mathbf{V}^T \tag{11}$$

Let $\tilde{\mathcal{S}}$ denote the point of $\mathcal{G}(N_\Phi, N_f)$ representing the reduced-order basis (yet to be found) adapted for the operating point $\tilde{\lambda}$, and let $\tilde{\mathcal{Y}}(t)$ denote the geodesic between $\mathcal{S}_0$ and $\tilde{\mathcal{S}}$ with $\mathcal{S}_0$ chosen as its origin; that is, the geodesic on $\mathcal{G}(N_\Phi, N_f)$ satisfying $\tilde{\mathcal{Y}}(0) = \mathcal{S}_0$ and $\tilde{\mathcal{Y}}(1) = \tilde{\mathcal{S}}$. Because the tangent space $\mathcal{T}_{\mathcal{S}_0}$ is a flat vector space and $\mathcal{S}_0$ is its origin, the data $((\log_{\mathcal{S}_0}\mathcal{S}_0 = 0), (\log_{\mathcal{S}_0}\mathcal{S}_1 = \dot{\mathcal{Y}}_0))$ can be interpolated in this plane to obtain the following approximation of the initial derivative of $\tilde{\mathcal{Y}}$:

$$\dot{\tilde{\mathcal{Y}}}_0 = \dot{\tilde{\mathcal{Y}}}(0) = \tilde{r}\dot{\mathcal{Y}}_0 \tag{12}$$

where

$$\tilde{r} = \frac{\tilde{s} - s_0}{s_1 - s_0} \tag{13}$$

can be described as the "reduced interpolation parameter." From Eq. (6) of Result 3, it follows that the representative matrix of $\dot{\tilde{\mathcal{Y}}}_0$ is

$$\tilde{\Gamma} = \tilde{r}\Gamma = \tilde{r}\mathbf{U}\tan^{-1}(\mathbf{\Sigma})\mathbf{V}^T = \mathbf{U}[\tilde{r}\tan^{-1}(\mathbf{\Sigma})]\mathbf{V}^T \tag{14}$$

From Eq. (8) of Result 4 and Eq. (14), it follows that the geodesic path on $\mathcal{G}(N_\Phi, N_f)$ with initial conditions $(\mathcal{Y}_0, \tilde{r}\dot{\mathcal{Y}}_0)$ is given by

$$\begin{aligned}\tilde{\mathcal{Y}}(t) = \operatorname{span}\{&\mathbf{\Psi}_0\mathbf{V}\cos[t\tilde{r}\tan^{-1}(\mathbf{\Sigma})] \\ &+ \mathbf{U}\sin[t\tilde{r}\tan^{-1}(\mathbf{\Sigma})]\} \qquad 0 \le t \le 1\end{aligned} \tag{15}$$

Therefore,

$$\tilde{\mathcal{Y}}(1) = \operatorname{span}\{\mathbf{\Psi}_0\mathbf{V}\cos[\tilde{r}\tan^{-1}(\mathbf{\Sigma})] + \mathbf{U}\sin[\tilde{r}\tan^{-1}(\mathbf{\Sigma})]\} \tag{16}$$

which, in view of Eqs. (6) and (8), implies

$$\tilde{\mathcal{Y}}(1) = \mathcal{Y}(\tilde{r}) \tag{17}$$

Since $\tilde{\mathcal{Y}}(1) = \tilde{\mathcal{S}}$, it follows that, in this case, the reduced-order basis adaptation method described so far interprets the geodesic originating at the point $\mathcal{S}_0$ associated with the value s_0 of the parameter s and ending at the point $\mathcal{S}_1$ associated with the value s_1 of s as the path on $\mathcal{G}(N_\Phi, N_f)$, which passes through all the reduced-order bases associated with $s \in [s_0, s_1]$. Hence, given the initial data $\dot{\mathcal{Y}}_0 = \log_{\mathcal{S}_0}\mathcal{S}_1$ [recall Eq. (2)], this adaptation procedure delivers for each value of $s \in [s_0, s_1]$ [recall Result 1 and Eqs. (12), (13), (15), and (17)] the reduced-order subspace

$$\mathcal{Y}(s) = \operatorname{Exp}_{\mathcal{Y}_0}\left[\left(\frac{s - s_0}{s_1 - s_0}\right)\dot{\mathcal{Y}}_0\right] \tag{18}$$

More specifically, given two matrices $\mathbf{\Psi}_0$ and $\mathbf{\Psi}_1$ associated with $\mathcal{S}_0$ and $\mathcal{S}_1$ (and therefore with s_0 and s_1) and representing two precomputed reduced-order bases, the proposed adaptation method constructs, in this case, for each value of the parameter $s \in [s_0, s_1]$ a reduced-order basis $\mathbf{\Psi}(s)$, as follows:

$$\begin{aligned}&\left(\mathbf{I} - \mathbf{\Psi}_0\mathbf{\Psi}_0^T\right)\mathbf{\Psi}_1\left(\mathbf{\Psi}_0^T\mathbf{\Psi}_1\right)^{-1} = \mathbf{U}\mathbf{\Sigma}\mathbf{V}^T \\ &\mathbf{\Psi}(s) = \mathbf{\Psi}_0\mathbf{V}\cos\left[\left(\frac{s - s_0}{s_1 - s_0}\right)\tan^{-1}(\mathbf{\Sigma})\right] \\ &\qquad + \mathbf{U}\sin\left[\left(\frac{s - s_0}{s_1 - s_0}\right)\tan^{-1}(\mathbf{\Sigma})\right]\end{aligned} \tag{19}$$

B. General Case

Here, the adaptation method presented in Sec. IV.A is extended to the case of an arbitrary number of precomputed reduced-order bases N_R and an arbitrary number of physical or modeling parameters per operating point N_p. This generalization is first described, then expressed as a four-step numerical algorithm.

To begin, one of the N_R precomputed reduced-order bases is chosen as a reference point of the Grassmann manifold of interest. Between this and each other precomputed and considered point of the manifold, a geodesic path is determined as described in Sec. IV.A. However, because the operating points of each pair of reference points and other precomputed points of the manifold do not necessarily differ by the value of a single parameter s, the geodesic that connects them does not necessarily represent in this case the variation of an appropriate reduced-order basis with the parameter s. Nevertheless, it is important to note that all such geodesics share the same initial position defined by the chosen reference point on the Grassmann manifold, but each has a different initial derivative.

Next, the initial derivatives, all of which belong to the tangent space at the chosen reference point, are interpolated using a preferred univariate or multivariate method, depending on whether the operating points contain a single parameter or multiple parameters.

Finally, the interpolated initial derivative is combined with the initial position defined by the chosen reference point to determine a new geodesic on the Grassmann manifold. The endpoint of this geodesic delivers the sought-after adapted reduced-order basis.

Remark 1. Interpolation in the tangent space to the Grassmann manifold at a reference point $\mathcal{T}_{\mathcal{S}}$ is simple because $\mathcal{T}_{\mathcal{S}}$ is a vector space. Indeed, the vector space property ensures the fact that the

interpolated initial derivative remains in $\mathcal{T}_{\mathcal{S}}$. In practice, each canonical coordinate of the matrix representing a point of $\mathcal{T}_{\mathcal{S}}$ can be interpolated independently. It is for this reason that methods involving interpolatory refinements on manifolds [36] or the computation of averages of affine-invariant point configurations [39] operate on tangent spaces to manifolds.

The aforementioned generalized adaptation method can be written as a four-step algorithm as follows.

Algorithm. Let $\{\mathcal{S}_i\}_{i=0}^{N_R-1}$ denote a set of N_Φ-dimensional subspaces of $\mathbb{R}^{N_f}$ associated with a set of different operating points $\{\lambda_i\}_{i=0}^{N_R-1}$. These subspaces are represented by their corresponding matrices $\{\mathbf{\Psi}_i \in \mathbb{R}^{N_f \times N_\Phi}\}_{i=0}^{N_R-1}$. The construction of a new N_Φ-dimensional subspace $\mathcal{S}_{N_R}$ associated with a new operating point λ_{N_R} can be obtained by interpolating the known subspaces $\{\mathcal{S}_i\}_{i=0}^{N_R-1}$ in four steps as follows.

Step 0. A point $\mathcal{S}_{i_0}$ of the manifold is chosen as a reference and origin point for the interpolation.

Step 1. The tangent space $\mathcal{T}_{\mathcal{S}_{i_0}}$ and those points among $\{\mathcal{S}_i\}_{i=0}^{N_R-1}$ which lie in a sufficiently small neighborhood of $\mathcal{S}_{i_0}$ are now considered. More specifically, each point $\mathcal{S}_i$ that is sufficiently close to $\mathcal{S}_{i_0}$ is mapped to a matrix Γ_i representing a point χ_i of $\mathcal{T}_{\mathcal{S}_{i_0}}$ using the logarithm map $\log_{\mathcal{S}_{i_0}}$. This can be written as

$$\left(\mathbf{I} - \mathbf{\Psi}_{i_0}\mathbf{\Psi}_{i_0}^T\right)\mathbf{\Psi}_i\left(\mathbf{\Psi}_{i_0}^T\mathbf{\Psi}_i\right)^{-1} = \mathbf{U}_i\mathbf{\Sigma}_i\mathbf{V}_i^T \qquad \text{(thin SVD)} \qquad (20)$$

$$\Gamma_i = \mathbf{U}_i \tan^{-1}(\mathbf{\Sigma}_i)\mathbf{V}_i^T \qquad (21)$$

Note that each χ_i point can be related to a geodesic, as $(\mathcal{S}_0, \chi_i)$ is the initial condition of the geodesic path on the manifold between $\mathcal{S}_0$ and $\mathcal{S}_i$ (for example, see Fig. 1).

Step 2. Each entry of the matrix Γ_{N_R} associated with the target operating point λ_{N_R} is computed by interpolating the corresponding entries of the matrices $\{\Gamma_i\} \in \mathbb{R}^{N_f \times N_\Phi}$ associated with the operating points $\{\lambda_i\}$. The choice of interpolation method depends on the number of physical parameters contained in each operating point N_p. When $N_p = 1$, a univariate (typically, a Lagrange type) interpolation method is chosen. Otherwise, a multivariate interpolation scheme (see, for example, [42,43]) is chosen.

Step 3. The matrix Γ_{N_R} representing $\chi_{N_R} \in \mathcal{T}_{\mathcal{S}_{i_0}}$ is mapped to a subspace $\mathcal{S}_{N_R}$ on the Grassmann manifold spanned by a matrix $\mathbf{\Psi}_{N_R}$ using the exponential map $\mathrm{Exp}_{\mathcal{S}_{i_0}}$. This can be written as

$$\Gamma_{N_R} = \mathbf{U}_{N_R}\mathbf{\Sigma}_{N_R}\mathbf{V}_{N_R}^T \qquad \text{(thin SVD)} \qquad (22)$$

$$\mathbf{\Psi}_{N_R} = \mathbf{\Psi}_{i_0}\mathbf{V}_{N_R}\cos(\mathbf{\Sigma}_{N_R}) + \mathbf{U}_{N_R}\sin(\mathbf{\Sigma}_{N_R}) \qquad (23)$$

The adaptation procedure specified in the preceding algorithm can be described as an interpolation method in a tangent space to a Grassmann manifold. It is graphically depicted in Fig. 2.

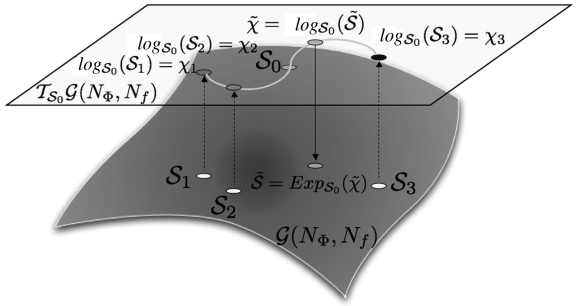

Fig. 2 Graphical description of the interpolation of four subspaces in a tangent space to a Grassmann manifold.

Remark 2. Because the logarithmic map $\log_S$ is defined in a neighborhood of $\mathcal{S} \in \mathcal{G}(N_\Phi, N_f)$, the preceding adaptation method is not sensitive, in principle, to the choice of the reference point $\mathcal{S}_{i_0}$ made in step 0. This is confirmed in practice, as will be shown in Sec. V.E.

C. Relation with Subspace Angle Interpolation Method

The authors have proven [44] that the subspace angle interpolation method [15,23,24,26] is identical to the interpolation in a tangent space to the Grassmann manifold of two and only two reduced-order bases. Hence, the interpolation method proposed in Sec. IV.B can be viewed as a higher-order extension of the subspace angle interpolation method, or in other terms, its generalization to an arbitrary number of ROMs.

D. Computational Complexity

Here, N_R denotes the number of ROMs participating in the adaptation procedure. As before, N_f denotes the dimension of the background high-order computational model, and all precomputed reduced-order bases are assumed to have the same dimension $N_\Phi \ll N_f$. Using this notation, the computational complexity of the method of interpolation in a tangent space to a Grassmann manifold described in Sec. IV.B is described next. For simplicity, the case $N_p = 1$ is assumed.

Step 1. $N_R - 1$ thin singular value decompositions are performed for a total asymptotic computational cost equal to $(N_R - 1)\times \mathcal{O}(N_f N_\Phi^2)$.

Step 2. In the case of a univariate interpolation, a Lagrange interpolation in the tangent space is performed at an asymptotic computational cost equal to $N_R \times \mathcal{O}(N_f N_\Phi)$.

Step 3. One thin SVD is performed at an asymptotic computational cost equal to $\mathcal{O}(N_f N_\Phi^2)$.

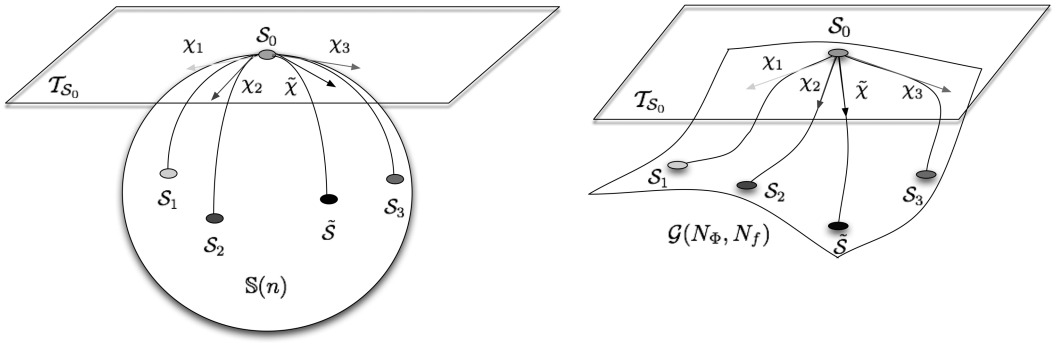

a) On the unit sphere manifold $\mathbb{S}(n)$ **b) On the Grassmann manifold $\mathcal{G}(N_\Phi, N_f)$**

Fig. 1 Riemannian manifolds, tangent planes, geodesics, initial positions, and initial derivatives.

Hence, the total asymptotic computational complexity of a univariate interpolation in a tangent space to a Grassmann manifold grows only as $N_R \times \mathcal{O}(N_f N_\Phi^2)$. Therefore, this complexity is a linear function of the size of the underlying higher-order computational model, which suggests that the proposed interpolation method is computationally efficient.

E. Reduced-Order Model Adaptation

After an adapted reduced-order basis is constructed as described in Sec. IV.B, an adapted ROM can be built using the same procedure that was used in the first place for constructing the precomputed ROMs from the precomputed reduced-order bases. Given that in most model reduction methods based on reduced-order bases, the phase of construction of the reduced-order basis dominates the total CPU time and is intrinsically expensive (for example, see [25]), and given the computational complexity results of Sec. IV.D, the ROM adaptation method proposed in this paper is a significantly more economical alternative to direct ROM reconstruction.

Remark 3. Because the proposed ROM adaptation method is essentially based on interpolation and all ROMs discussed in this paper are based on the POD method, the words "adaptation" and "interpolation" are used interchangeably throughout the remainder of this paper and imply the same thing whether used in front of the words POD basis or the word ROM.

V. Application to CFD-Based Computational Aeroelasticity

In this section, the proposed ROM adaptation method is illustrated with its application to the CFD-based aeroelastic analysis of two fighter aircraft configurations: a clean wing F-16 Block 40 configuration and a limit-cycle F/A-18 configuration. In both cases, the POD method [45] (sometimes also referred to as the principal component analysis or the Karhunen–Loeve method) is chosen as the underlying model reduction method. All computations are performed within the CFD-based aeroelastic code AERO [46,47].

First, a brief overview of the adopted high-fidelity aeroelastic computational model and its POD-based, reduced-order counterpart are given. Then, the proposed ROM adaptation method is specialized to the target application. Next, its performance is assessed for each of the two fighter applications. Finally, the robustness of the proposed ROM adaptation with respect to the choice of the reference precomputed reduced-order basis and its relationship to the subspace angle interpolation method are highlighted.

A. Linearized High-Fidelity and POD-Based Aeroelastic Reduced-Order Models

Although computational aeroelasticity involves the coupling of fluid and structural subsystem models, model reduction is performed here for each of them separately following the approach advocated in [23,25]. This decoupled reduced-order modeling approach has several advantages. First, it allows the use of the most suitable ROM technique for each individual discipline. Second, it allows formulating the fluid model in nondimensional form, thereby making its reduced-order basis independent of the freestream pressure and density. The latter property makes the adaptation of the resulting aeroelastic ROM to a variation of altitude a trivial task.

A high-fidelity, CFD-based, nonlinear aeroelastic system can be nondimensionalized and linearized around an equilibrium point to obtain the following form of the semidiscrete system of equations governing its fluid subsystem (see, for example, [23–26,48]):

$$\bar{\mathbf{w}}_{,\tau} + \bar{\mathbf{H}}\,\bar{\mathbf{w}} + \bar{\mathbf{B}}\,\bar{\mathbf{y}} = 0 \tag{24}$$

Here, the bar notation designates a nondimensional quantity, $\mathbf{w}$ denotes the fluid state vector in conservation variables, "$,\tau$" designates the partial derivative with respect to the nondimensional time τ, $\bar{\mathbf{H}} \in \mathbb{R}^{N_f \times N_f}$ is the first-order term of the Taylor expansion of the (nondimensional) CFD flux function, and N_f denotes the dimension of the high-fidelity fluid subsystem model. In this work, all flows are assumed to be inviscid and therefore $\bar{\mathbf{H}}$ is associated with the linearization of the Euler equations. Also in Eq. (24), $\bar{\mathbf{B}} \in \mathbb{R}^{N_f \times 2N_s}$ denotes the coupling matrix with the structural model that is part of the aeroelastic system of interest, N_s denotes the dimension of the structural model, and $\bar{\mathbf{y}} \in \mathbb{R}^{2N_s}$ denotes its state vector in space-state form. Hence,

$$\bar{\mathbf{y}} = \begin{bmatrix} \dot{\bar{\mathbf{u}}} \\ \bar{\mathbf{u}} \end{bmatrix} \tag{25}$$

where a dot designates the dimensional time derivative, and $\bar{\mathbf{u}} \in \mathbb{R}^{N_s}$ and $\dot{\bar{\mathbf{u}}} \in \mathbb{R}^{N_s}$ denote the vectors of structural displacements and velocities, respectively. For a pure fluid problem, $\bar{\mathbf{B}}\,\bar{\mathbf{y}}$ is set to $\mathbf{0}$ in Eq. (24).

The fluid ROM associated with the higher-order computational fluid model, as described before, is represented here by the following two mathematical entities:

1) A full column rank matrix $\mathbf{\Phi} \in \mathbb{R}^{N_f \times N_\Phi}$ whose columns represent the basis of a subspace and which satisfies the orthogonality condition

$$\mathbf{\Phi}^T \mathbf{\Phi} = \mathbf{I}_{N_\Phi} \tag{26}$$

where $N_\Phi \ll N_f$ and $\mathbf{I}_{N_\Phi}$ denotes the identity matrix of dimension N_Φ. In this work, $\mathbf{\Phi}$ is obtained by applying the POD method to Eq. (24) in the frequency domain, as described in many references including [7–9,14,25].

2) The reduced-order form of Eq. (24), which can be written as

$$(\bar{\mathbf{w}}_r)_{,\tau} - \bar{\mathbf{H}}_r \bar{\mathbf{w}}_r + \bar{\mathbf{B}}_r \bar{\mathbf{y}} = \mathbf{0} \tag{27}$$

where $\bar{\mathbf{H}}_r \in \mathbb{R}^{N_\Phi \times N_\Phi}$ denotes the projection of $\bar{\mathbf{H}}$ onto the subspace spanned by the columns of $\mathbf{\Phi}$, $\bar{\mathbf{w}}_r$ denotes the projection onto the same subspace of the underlying nondimensional full-order fluid state vector; that is,

$$\bar{\mathbf{w}}_r = \mathbf{\Phi}^T \bar{\mathbf{w}} \tag{28}$$

the T superscript designates the transpose of a quantity, and $\bar{\mathbf{B}}_r \in \mathbb{R}^{N_\Phi \times 2N_s}$ denotes the projection of $\bar{\mathbf{B}}$ onto the subspace spanned by the columns of $\mathbf{\Phi}$.

The linear ROM chosen for modeling the dynamics of the structural subsystem is based on the classical model reduction. Hence, it is represented here by the following three mathematical entities:

1) A set of N_m natural modes of the "dry" structure are represented by the matrix of eigenvectors $\mathbf{X} \in \mathbb{R}^{N_s \times N_m}$.

2) The corresponding matrix of eigenvalues (squares of natural circular frequencies) $\mathbf{\Omega}^2 \in \mathbb{R}^{N_m \times N_m}$.

3) The reduced-order form of the governing equation of dynamic equilibrium which can be written as (see, for example, [23,24,26])

$$\mathbf{I}_{N_m} \ddot{\mathbf{u}}_m + \mathbf{\Omega}^2 \mathbf{u}_m = \mathbf{X}^T \mathbf{P} \bar{\mathbf{w}} \tag{29}$$

where $\mathbf{u}_m$ denotes the vector of generalized (modal) coordinates,

$$\mathbf{P} = \frac{\partial \mathbf{f}^{\text{ext}}}{\partial \bar{\mathbf{w}}}(\mathbf{w}_o, \mathbf{u}_o) \tag{30}$$

$\mathbf{f}^{\text{ext}}$ denotes the vector of external forces (including the aerodynamic forces) acting on the structure, and the subscript o designates the chosen equilibrium (or linearization) point.

Hence, the linear aeroelastic ROM chosen in this work can be fully described by the following:

1) The matrices $\mathbf{\Phi} \in \mathbb{R}^{N_f \times N_\Phi}$, $\mathbf{X} \in \mathbb{R}^{N_s \times N_m}$, and $\mathbf{\Omega}^2 \in \mathbb{R}^{N_m \times N_m}$ as defined earlier.

2) The coupled system of governing equations

$$\begin{aligned} (\bar{\mathbf{w}}_r)_{,\tau} - \bar{\mathbf{H}}_r \bar{\mathbf{w}}_r + \bar{\mathbf{B}}_r \bar{\mathbf{y}}_r &= \mathbf{0} \\ \mathbf{I}_{N_m} \ddot{\mathbf{u}}_m + \mathbf{\Omega}^2 \mathbf{u}_m &= \mathbf{X}^T \mathbf{P} \bar{\mathbf{w}} \end{aligned} \tag{31}$$

where

$$\bar{\mathbf{y}}_r = \begin{bmatrix} \mathbf{X}\dot{\bar{\mathbf{u}}}_m \\ \mathbf{X}\bar{\mathbf{u}}_m \end{bmatrix} \tag{32}$$

B. Aeroelastic ROM Adaptation

Let M_∞ denote the freestream Mach number. For simplicity, but without any loss of generality, this physical parameter is the only parameter considered in all following sections for defining an operating point λ. Its significance is emphasized by noting that Eq. (27), which governs the ROM of the fluid subsystem, is obtained by linearizing the Euler equations around this freestream condition. Furthermore, it is assumed that the following data are either given or precomputed: 1) $N_R > 1$ linear fluid ROMs of the same dimension represented by their reduced-order bases constructed by the POD method at N_R different operating points $\lambda_i = M_{\infty_i}$ with $M_{\infty_i} \neq M_{\infty_j}$ for $i \neq j$ and $M_{\infty_i} \in \mathcal{M}$; 2) a single linear structural ROM.

Then, the objective is to exploit the aforementioned data to rapidly construct a linear aeroelastic ROM at a specified operating point $\lambda_l = M_{\infty_l}$ with $M_{\infty_l} \notin \mathcal{M}$, using the adaptive method described in Sec. IV.

To complete the description of this adaptation method, only the interpolation algorithm to be applied in the tangent space to the Grassmann manifold at the chosen reference point needs be specified. For this problem, the simple Lagrangian approximation scheme is chosen for this purpose. Therefore, after a reference reduced-order basis associated with a reference Mach number $M_{\infty_{i_0}}$ is chosen and denoted here by $\mathcal{S}_0 \in \mathcal{G}(N_\Phi, N_f)$, the data $\Gamma_i(M_{\infty_i})$ in the tangent space to $\mathcal{G}(N_\Phi, N_f)$ at $\mathcal{S}_0$ representing the initial derivatives of the trajectories $\mathcal{Y}_i$ associated with the parameters $\lambda_i = M_{\infty_i}$ is interpolated as follows [note that $\Gamma_{i_0}(M_{\infty_{i_0}}) = 0$]

$$\Gamma(M_{\infty_l}) = \sum_{i=0}^{N_R-1} \left(\prod_{j \neq i} \frac{M_{\infty_l} - M_{\infty_j}}{M_{\infty_i} - M_{\infty_j}} \right) \Gamma_i(M_{\infty_i}) \tag{33}$$

Then, using Eqs. (22) and (23), the new reduced-order basis $\mathbf{\Psi}_{N_R}$ associated with the new operating point $\lambda_l = M_{\infty_l}$ with $M_{\infty_l} \notin \mathcal{M}$ is constructed. Finally, given the decoupled approach chosen here for building the aeroelastic ROM and the adoption of classical model reduction for modeling the linear dynamics of the structural subsystem, it remains only to construct the matrices $\bar{\mathbf{H}}_r$ and $\bar{\mathbf{B}}_r$ to complete the construction of the aeroelastic ROM associated with the new operating point λ_l. This construction requires the availability of the linearized operator $\mathbf{H}$ around the point M_{∞_l}, and the calculation of the product $\mathbf{\Psi}_{N_R}^T \mathbf{H} \mathbf{\Psi}_{N_R}$. The latter calculation is inexpensive. The former one implies either the calculation of a new steady state (which is required anyway by the direct reconstruction of a new ROM at the new operating point λ_l and consumes only a small fraction of the cost of this reconstruction) or the availability in the database of this steady state.

C. Adaptation of F-16 ROMs to New Freestream Data in Transonic Regime

The considered high-fidelity aeroelastic computational model of an F-16 Block 40 aircraft in clean wing configuration consists of: 1) an FE structural model with 168,799 DOF built with bar, beam, solid, plate, and shell, metallic, and composite elements, and 2) an unstructured CFD (Euler) grid with 403,919 vertices and more than two million DOF (Fig. 3).

First, the lack of robustness of a POD-based aeroelastic ROM of this aircraft with respect to a variation of the freestream Mach number is highlighted. For this purpose, a single POD basis is constructed at the trimmed flight condition ($M_{\infty_2} = 0.710$, $\alpha_2 = 3.2$ deg). The projection on this reduced-order basis of the linearization of the fluid model at this flight condition is combined with a modal representation of the aforementioned high-fidelity FE structural model to obtain an aeroelastic ROM of dimension 69. Then, this ROM is used to predict the aeroelastic response of the F-16 aircraft to an initial excitation at three different trimmed flight conditions: ($M_{\infty_1} = 0.611$, $\alpha_1 = 4.5$ deg), ($M_{\infty_2} = 0.710$, $\alpha_2 = 3.2$ deg) and ($M_{\infty_3} = 0.799$, $\alpha_3 = 3.0$ deg). The obtained lift time histories are reported in Fig. 4 and compared with their counterparts predicted using the linearization of the high-fidelity aeroelastic model at the same considered flight conditions. The reader can observe that when applied at ($M_{\infty_1} = 0.611$, $\alpha_1 = 4.5$ deg), the aeroelastic ROM constructed at ($M_{\infty_2} = 0.710$, $\alpha_2 = 3.2$ deg) is unstable (the X symbol in Fig. 4 is used to highlight the breaking of the time-dependent computation because of a numerical instability that causes some density and/or pressure values to become negative). When applied at ($M_{\infty_3} = 0.799$, $\alpha_3 = 3.0$ deg), the aforementioned aeroelastic ROM is weakly unstable and in any case totally inaccurate.

Next, the potential of the new interpolation method is assessed. To this effect, two different sets of numerical simulations are performed. In the first set, four POD bases of dimension 90 are precomputed at the flight conditions ($M_{\infty_1} = 0.650$, $M_{\infty_2} = 0.710$, $M_{\infty_3} = 0.850$, and $M_{\infty_4} = 0.875$) and stored in a database. In all four cases, the freestream angle of attack is set to $\alpha = 3.0$ deg. The method of interpolation in a tangent space to the Grassmann manifold is then applied to construct a new POD basis at the flight condition $M_\infty = 0.799, \alpha = 3.0$ deg by interpolating 1) the precomputed POD bases associated with the three operating points M_{∞_1}, M_{∞_2}, and M_{∞_3}, and 2) the precomputed POD bases associated with the four operating points $M_{\infty_1}, M_{\infty_2}, M_{\infty_3}$, and M_{∞_4}. Figure 5 reports the lift time histories obtained using both interpolated ROMs, a POD-based aeroelastic ROM of the same dimension that is directly constructed at the new target flight condition, and the linearization at the same target flight condition ($M_\infty = 0.799$ and $\alpha = 3.0$ deg) of the high-fidelity nonlinear aeroelastic model. The reader can observe that, although the aeroelastic ROM obtained by interpolating the three first precomputed ROMs tracks well the lift time history produced by the ROM directly constructed at the new target flight condition, there is an increasing offset between the two results after $t = 0.3$ s. However, the aeroelastic ROM obtained by interpolating all four precomputed aeroelastic ROMs reproduces perfectly both lift time histories produced by the ROM directly constructed at the new target flight condition, and that generated by the linearized high-fidelity aeroelastic model.

In a second experiment, two POD bases of dimension 60 are first precomputed at the trimmed flight conditions ($M_{\infty_1} = 0.923$, $\alpha_1 = 1.4$ deg) and ($M_{\infty_2} = 1.114, \alpha_2 = 1.5$ deg) and combined with

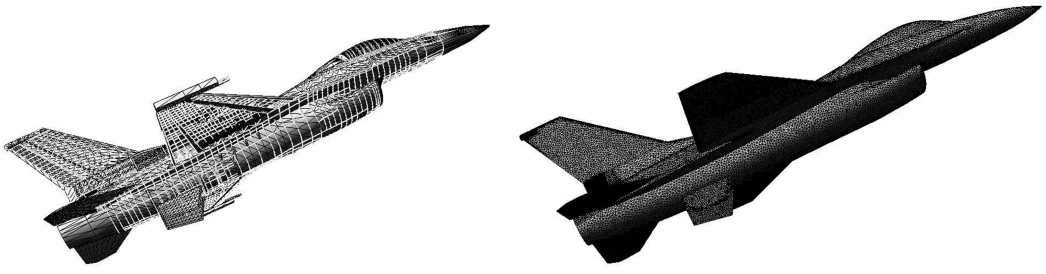

a) FE structural model b) CFD surface grid

Fig. 3 High-fidelity aeroelastic model of an F-16 configuration.

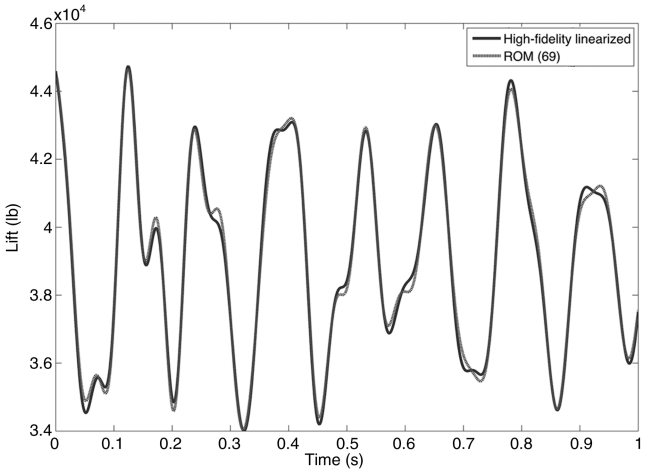

a) $M_{\infty_2} = 0.710$, $\alpha_2 = 3.2°$

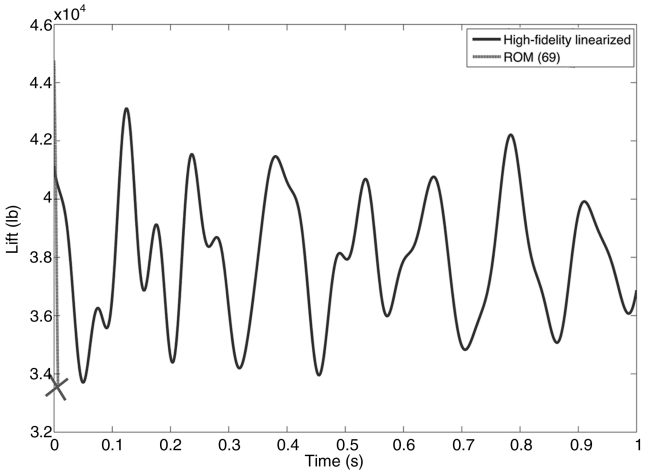

b) $M_{\infty_1} = 0.611$, $\alpha_1 = 4.5°$

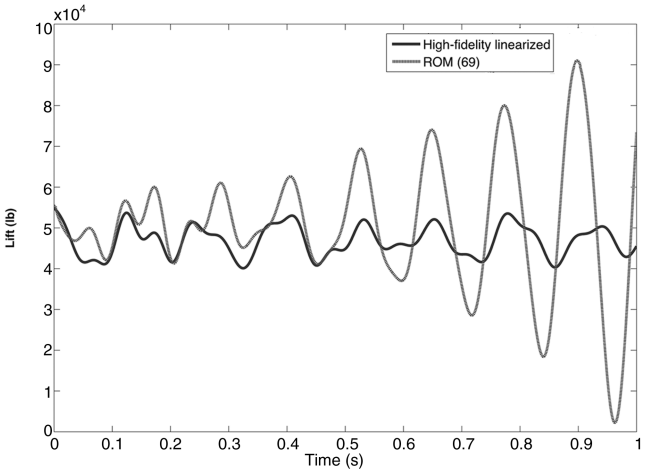

c) $M_{\infty_3} = 0.799$, $\alpha_3 = 3.0°$

Fig. 4 Comparison of the lift time histories predicted for an F-16 configuration at ($M_{\infty_1} = 0.611$, $\alpha_1 = 4.5\,\text{deg}$), ($M_{\infty_2} = 0.710$, $\alpha_2 = 3.2\,\text{deg}$), and ($M_{\infty_3} = 0.799$, $\alpha_3 = 3.0\,\text{deg}$) using a) the linearization of the high-fidelity models at the considered flight conditions, and b) the ROM constructed at (M_{∞_2}, α_2).

the aforementioned structural modal representation. In [26], the subspace angle interpolation method was applied to interpolate these reduced-order bases in the interval $M_\infty \in [0.923, 1.114]$ and the corresponding trim angles of attack. It was found and reported that, in this case, the subspace angle interpolation method fails to construct a stable interpolated POD at each of the two operating points $M_\infty = 1.072$ and $M_\infty = 1.031$. Consequently, an intermediate POD basis

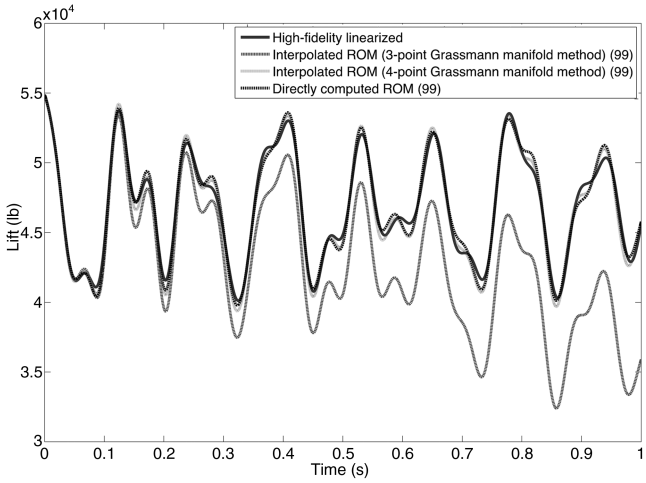

Fig. 5 Comparison of the lift time histories of the F-16 configuration at ($M_\infty = 0.799$, $\alpha = 3.0\,\text{deg}$) produced by a) ROM obtained by interpolating in a tangent space to a Grassmann manifold three aeroelastic ROMs precomputed at $M_{\infty_1} = 0.65$, $M_{\infty_2} = 0.71$, and $M_{\infty_3} = 0.85$; b) ROM obtained by adapting four aeroelastic ROMs precomputed at $M_{\infty_1} = 0.65$, $M_{\infty_2} = 0.71$, $M_{\infty_3} = 0.85$, and $M_{\infty_4} = 0.875$ using the same interpolation method; c) aeroelastic ROM directly constructed at (M_∞, α); and d) linearization of a high-fidelity aeroelastic model at (M_∞, α).

was precomputed at $M_{\infty_3} = 1.031$ and its trim angle of attack, $\alpha_3 = 1.4\,\text{deg}$, and piecewise linear interpolations were reattempted in the same interval $M_\infty \in [0.923, 1.114]$ using the subspace angle interpolation method (see [26] for details). The obtained results, which were first reported in [26], are included here in Fig. 6 as a reference point. The reader can observe that, in this case, the piecewise linearly interpolated ROMs using the subspace angle interpolation method track relatively well the variation of the first torsional aeroelastic damping ratio with the freestream Mach number, except for $M_\infty = 0.990$.

Here, a different attempt at interpolating the three aforementioned precomputed POD bases in the same transonic interval $M_\infty \in [0.923, 1.114]$ is performed using the proposed method of interpolation in a tangent space to a Grassmann manifold. Indeed, unlike the subspace angle interpolation method, the more general method proposed in this paper allows higher-order approximations

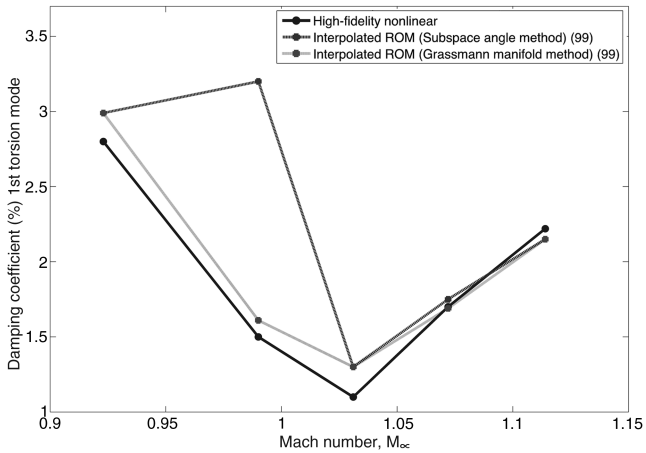

Fig. 6 Comparison of the first torsional aeroelastic damping coefficients of the F-16 configuration predicted in the transonic interval $M_\infty \in [0.923, 1.114]$ using a) subspace angle interpolation method applied to the piecewise linear interpolation of three aeroelastic ROMs precomputed at the three trimmed flight conditions ($M_{\infty_1} = 0.923$, $\alpha_1 = 1.4\,\text{deg}$), ($M_{\infty_2} = 1.031$, $\alpha_2 = 1.4\,\text{deg}$), and ($M_{\infty_3} = 1.114$, $\alpha_3 = 1.5\,\text{deg}$); b) higher-order method of interpolation in a tangent space to a Grassmann manifold applied to the same three precomputed ROMs; and c) high-fidelity nonlinear aeroelastic model.

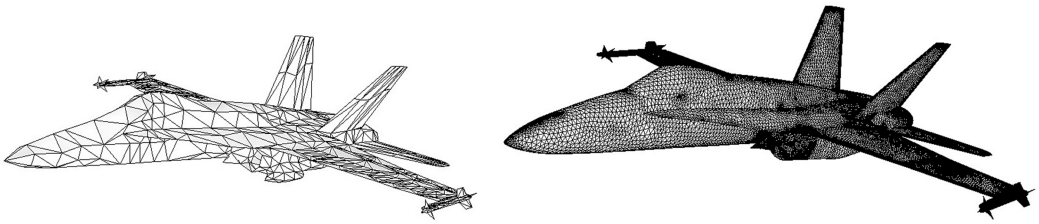

a) FE structural model **b) CFD surface grid**

Fig. 7 High-fidelity aeroelastic model of an F-18/A configuration.

and can interpolate in one shot all three POD bases precomputed at ($M_{\infty_1} = 0.923$, $\alpha_1 = 1.4$ deg), ($M_{\infty_2} = 1.114$, $\alpha_2 = 1.5$ deg), and ($M_{\infty_3} = 1.031$, $\alpha_3 = 1.4$ deg). Figure 6 shows that, in this case, the new ROM adaptation method proposed in this paper delivers more accurate results in the entire transonic interval $M_\infty \in [0.923, 1.114]$.

D. Adaptation of F/A-18 ROMs to New Freestream Data

The high-fidelity aeroelastic computational model of an F-18/A configuration with tip missiles considered here consists of an 11,290 DOF FE structural model and an unstructured CFD (Euler) grid with 716,619 vertices and thus more than three and a half million DOF (Fig. 7). Four POD bases of dimension 40 are precomputed at the following freestream Mach numbers: $M_{\infty_1} = 0.5$, $M_{\infty_2} = 0.7$, $M_{\infty_3} = 0.75$, and $M_{\infty_4} = 0.8$. In all four cases, the angle of attack is set to $\alpha = 4.85$ deg. Then, each reduced-order POD basis is coupled with a modal representation of dimension 11 of the high-fidelity FE structural model to construct at each considered flight condition an aeroelastic ROM of dimension 51.

First, both the method of interpolation in a tangent space to a Grassmann manifold and that of direct interpolation of basis vectors are applied to interpolate the four precomputed aeroelastic ROMs and generate a new ROM capable of operating at ($M_\infty = 0.725$, $\alpha = 4.85$ deg). Figure 8 reports the lift time histories obtained when applying the Mach-interpolated aeroelastic ROMs using both interpolation methods to the solution of a given aeroelastic response problem. The reader can observe that the interpolated ROM using the adaptation method proposed in this paper performs well, whereas that obtained by direct interpolation of the POD basis vectors diverges after a few time-steps.

Next, the method of interpolation in a tangent space to a Grassmann manifold is applied to interpolate 1) two of the POD bases whose operating points are closest to that of the new target flight condition; that is, the POD bases corresponding to $M_{\infty_2} = 0.7$ and $M_{\infty_3} = 0.75$, and 2) all four precomputed POD bases. Figure 9 reports the lift time histories obtained using both interpolated ROMs, a POD-based aeroelastic ROM of the same dimension that is directly constructed at the new target flight condition, and the linearization at the same target flight condition ($M_\infty = 0.725$ and $\alpha = 4.85$ deg) of the high-fidelity nonlinear aeroelastic model. The reader can observe that the aeroelastic ROM obtained by interpolating all four precomputed aeroelastic ROMs reproduces almost perfectly the lift time history produced by the ROM directly constructed at the new target flight condition, and that this lift time history correlates well with that of the linearized high-fidelity aeroelastic model. The reader can also observe that, although the results obtained by interpolating only two of the precomputed aeroelastic ROMs are less than perfect, they highlight the feasibility of applying adaptively the proposed ROM interpolation method. Indeed, as with most interpolation methods, the proposed ROM adaptation method can be applied to interpolate an increasing number of ROMs that are stored in a database until the target simulation result is converged.

E. Robustness with Respect to Choice of Reference Reduced-Order Basis

In Remark 2 of Sec. IV.B, it was stated that the proposed ROM adaptation method is robust with respect to the choice of the reference point where the tangent to the relevant Grassmann manifold is constructed, as long as all precomputed ROMs to be interpolated are chosen in the neighborhood of the reference point. This statement is supported here by one example, namely, the problem of interpolating all four precomputed F-18/A aeroelastic

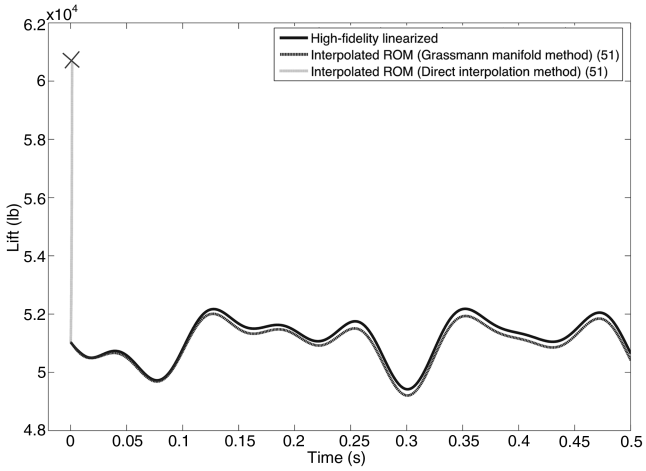

Fig. 8 Comparison of the lift time histories of an F/A-18 configuration at ($M_\infty = 0.725$, $\alpha = 4.85$ deg) produced by a) ROM obtained by interpolating in a tangent space to a Grassmann manifold, four aeroelastic ROMs precomputed at $M_{\infty_1} = 0.5, M_{\infty_2} = 0.7, M_{\infty_3} = 0.75$, and $M_{\infty_4} = 0.8$; b) ROM associated with the direct interpolation of the POD bases precomputed at the same four different Mach numbers; and c) linearization of a high-fidelity aeroelastic model at the same target flight condition.

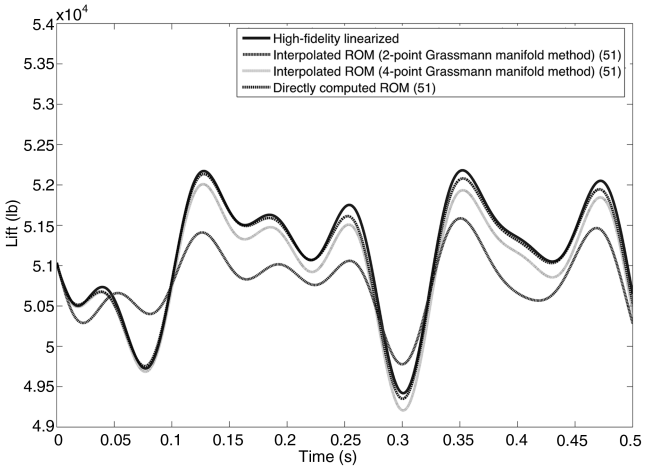

Fig. 9 Comparison of the lift time histories of an F/A-18 configuration at ($M_\infty = 0.725$, $\alpha = 4.85$ deg) produced by a) ROM obtained by interpolating in a tangent space to a Grassmann manifold two aeroelastic ROMs precomputed at $M_{\infty_2} = 0.7$ and $M_{\infty_3} = 0.75$; b) ROM obtained by adapting four aeroelastic ROMs precomputed at $M_{\infty_1} = 0.5$, $M_{\infty_2} = 0.7$, $M_{\infty_3} = 0.75$, and $M_{\infty_4} = 0.8$ using the same interpolation method; c) aeroelastic ROM directly constructed at (M_∞, α); and d) linearization of a high-fidelity aeroelastic model at (M_∞, α).

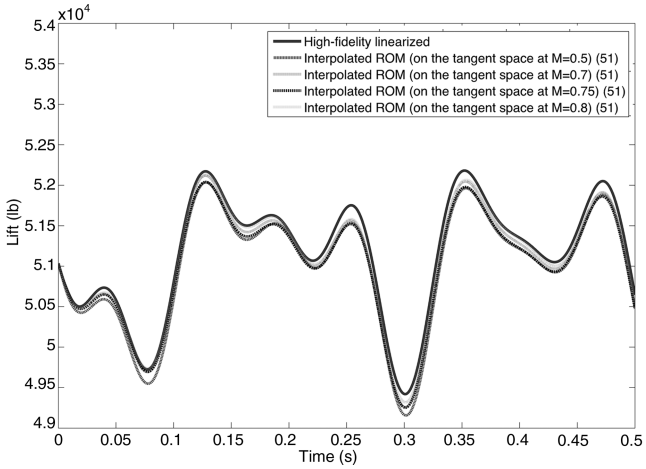

Fig. 10 Comparison of the F-18/A lift time histories produced by the four ROMs of dimension 51 obtained by interpolating at ($M_\infty = 0.725$, $\alpha = 4.85\,\text{deg}$) the same four precomputed POD bases but in four different tangent spaces to the same Grassmann manifold.

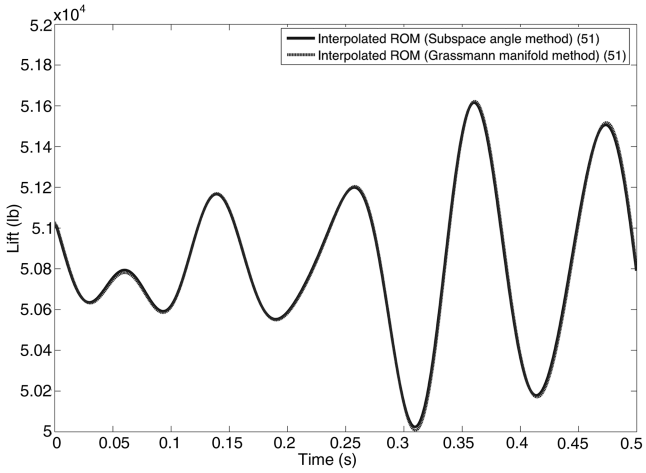

Fig. 11 Comparison of the lift time histories produced by the F-18/A aeroelastic ROMs at ($M_\infty = 0.725, \alpha = 4.85\,\text{deg}$) obtained using both of the subspace and Grassmann interpolation methods.

ROMs introduced in Sec. V.D to construct a new aeroelastic ROM at the operating point ($M_\infty = 0.725$, $\alpha = 4.85\,\text{deg}$).

For this purpose, the method of interpolation in a tangent space to the Grassmann manifold is applied four times to interpolate the four aforementioned precomputed ROMs and produce an aeroelastic ROM that can operate at ($M_\infty = 0.725$, $\alpha = 4.85\,\text{deg}$). Each time, one of the precomputed POD bases is chosen as a different reference point. Then, each of the four different aeroelastic ROMs obtained by interpolation is used to solve the same aeroelastic response problem associated with an initial perturbation of an aeroelastic state of equilibrium. The four computed lift time histories are reported in Fig. 10 and contrasted with the lift time history obtained using the linearization at the same operating point of the high-fidelity nonlinear aeroelastic model. The reader can observe that all four lift time histories are nearly identical. This result supports the statement made about the robustness with respect to the chosen reference point of the proposed method of interpolation in a tangent space to a Grassmann manifold.

F. Relation to Subspace Angle Interpolation Method

In Sec. IV.C, it was mentioned that it was recently proved that the subspace angle interpolation method corresponds to the particular case of a two-point Grassmann interpolation method [44]. This statement is illustrated here by the following example. Two POD bases corresponding to ($M_{\infty_1} = 0.7$, $\alpha = 4.85\,\text{deg}$) and ($M_{\infty_2} = 0.75$, $\alpha = 4.85\,\text{deg}$) are adapted using both the subspace angle interpolation method and the method of interpolation in a tangent space to a Grassmann manifold to generate a new POD basis for the operating point ($M_\infty = 0.725$, $\alpha = 4.85\,\text{deg}$). Figure 11 shows that the lift time histories obtained by applying the Mach-interpolated aeroelastic ROMs produced by both interpolation methods to the solution of a given aeroelastic response problem are identical.

VI. Conclusions

There are three important facts to keep in mind when considering a linear reduced-order model: 1) it is typically constructed at a given operating point that can depend on multiple physical or modeling parameters, 2) its construction can be CPU intensive, and 3) once constructed, it often lacks robustness with respect to changes in the operating point. Hence, the routine usage of a ROM-based computational technology in applications such as design, analysis, and test operations calls for a means for adapting a set of precomputed ROMs to a new, "last minute," operating point. To this effect, this paper has presented a new ROM adaptation method based on interpolation in a tangent space to a Grassmann manifold. This method is equally applicable to all ROMs that are based on projection schemes. The accuracy of this ROM adaptation method was demonstrated for the adaptation of a set of precomputed aeroelastic ROMs to new freestream data, thereby avoiding the expensive cost of reconstructing aeroelastic ROMs for new freestream Mach numbers. For this purpose, two realistic aircraft configurations were considered: an F-16 Block 40 fighter with clean wings in the transonic regime, and an F-18/A fighter with tip missiles. Excellent results were demonstrated in both cases. The proposed ROM adaptation method is expected to pave the way for a new computational strategy based on ROM databases. Indeed, assuming that a minimal set of reduced-order bases has been precomputed for a number of preselected operating points and stored in a database, when a request is formulated for a ROM at an operating point that is not available in this database, the proposed ROM adaptation method is a promising technology for enabling the computation in near real time of a new ROM associated with the desired operating point.

Acknowledgments

This material is based upon work supported partially by the U.S. Air Force Office of Scientific Research under Grant FA9550-06-01-0247, and partially by the National Science Foundation under Grant CNS-0540419. Any opinions, findings, and conclusions or recommendations expressed in this material are those of the authors and do not necessarily reflect the views of the U.S. Air Force Office of Scientific Research or the National Science Foundation. The authors wish to thank Thuan Lieu for his contribution to the application sections of this paper and Julien Cortial for his contribution to establishing the relationship between the subspace angle and Grassmann manifold interpolation methods.

References

[1] Woon, S. K., and Marshall, S. A., "Design of Multivariable Control Systems Using Reduced-Order Models," *Electronics Letters*, Vol. 11, No. 15, 1975, pp. 341–342. doi:10.1049/el:19750261

[2] LeGresley, P. A., and Alonso, J., "Airfoil Design Optimization Using Reduced Order Models Based on Proper Orthogonal Decomposition," AIAA Paper 00-25450, 2000.

[3] Lall, S., Mardsen, J. E., and Glavaski, S., "Subspace Approach to Balanced Truncation for Model Reduction of Nonlinear Control Systems," *International Journal of Robust and Nonlinear Control*, Vol. 12, No. 6, 2002, pp. 519–535. doi:10.1002/rnc.657

[4] Michopoulos, J., Tsompanopoulou, P., Houstis, E., Rice, J., Farhat, C., Lesoinne, M., and Lechenault, F., *DDEMA: a Data-Driven Environment for Multiphysics Applications*, edited by P. M. A. Sloot, D. Abramson, A. Bogdanov, J. J. Dongarra, A. Zomaya, and Y.

Gorbache, Lecture Notes in Computer Science, 2660, Pt. 4, Springer–Verlag, Heidelberg, Germany, 2003, pp. 309–318.
[5] Cortial, J., Farhat, C., Rajashekhar, M., and Guibas, L., *Compressed Sensing and Time-Parallel Reduced-Order Modeling for Structural Health Monitoring using a DDDAS*, Lecture Notes in Computer Science, Vol. 11, Springer–Verlag, Heidelberg, Germany, No. 4487, 2007, pp. 1171–1179.
[6] Romanowski, M. C., "Reduced Order Unsteady Aerodynamic and Aeroelastic Models Using Karhunen-Loeve Eigenmodes," *6th AIAA/USAF/NASA/ISSMO Symposium on Multidisciplinary Analysis and Optimization*, AIAA Paper 1996-3981, Sept. 1996.
[7] Kim, T., "Frequency-Domain Karhunen–Loeve Method and Its Application to Linear Dynamic Systems," *AIAA Journal*, Vol. 36, No. 11, 1998, pp. 2117–2123.
[8] Hall, K. C., Thomas, J. P., and Dowell, E. H., "Reduced-Order Modelling of Unsteady Small-Disturbance Flows Using a Frequency Domain Proper Orthogonal Decomposition Technique," AIAA Paper 99-16520, 1999.
[9] Hall, K. C., Thomas, J. P., and Dowell, E. H., "Proper Orthogonal Decomposition Technique for Transonic Unsteady Aerodynamic Flows," *AIAA Journal*, Vol. 38, No. 2, Oct. 2000, pp. 1853–1862.
[10] Willcox, K., and Peraire, J., "Balanced Model Reduction via the Proper Orthogonal Decomposition," *AIAA Journal*, Vol. 40, No. 11, Nov. 2002, pp. 2323–30.
[11] Kim, T., and Bussoletti, J. E., "Optimal Reduced-Order Aeroelastic Modeling Based on a Response-Based Modal Analysis of Unsteady CFD Models," AIAA Paper 2001-1525, 2001.
[12] Kim, T., Hong, M., Bhatia, K. B., and SenGupta, G., "Aeroelastic Model Reduction for Affordable Computational Fluid Dynamics-Based Flutter Analysis," *AIAA Journal*, Vol. 43, No. 12, Dec. 2005, pp. 2487–2495.
doi:10.2514/1.11246
[13] Epureanu, B. I., "Parametric Analysis of Reduced Order Models of Viscous Flows in Turbomachinery," *Journal of Fluids and Structures*, Vol. 17, No. 7, 2003, pp. 971–982.
doi:10.1016/S0889-9746(03)00044-6
[14] Thomas, J. P., Dowell, E. H., and Hall, K. C., "Three-Dimensional Transonic Aeroelasticity Using Proper Orthogonal Decomposition-Based Reduced Order Models," *Journal of Aircraft*, Vol. 40, No. 3, 2003, pp. 544–551.
[15] Lieu, T., and Lesoinne, M., "Parameter Adaptation of Reduced Order Models for Three-Dimensional Flutter Analysis," AIAA Paper 2004-0888, 2004.
[16] Cizmas, P. G. A., and Palacios, A., "Proper Orthogonal Decomposition of Turbine Rotor-Stator Interaction," *Journal of Propulsion and Power*, Vol. 19, No. 2, March 2003, pp. 268–281.
[17] Silva, W., "Identification of Nonlinear Aeroelastic Systems Based on the Volterra Theory: Progress and Opportunities," *Nonlinear Dynamics*, Vol. 39, Nos. 1–2, Jan. 2005, pp. 25–62.
doi:10.1007/s11071-005-1907-z
[18] Silva, W. A., and Bartels, R. E., "Development of Reduced-Order Models for Aeroelastic Analysis and Flutter Prediction Using the CFL3Dv6.0 Code," *Journal of Fluids and Structures*, Vol. 19, No. 6, July 2004, pp. 729–745.
doi:10.1016/j.jfluidstructs.2004.03.004
[19] Spitler, J. E., "Initial Studies of Low-Order Turbulence Modeling of the Wind Turbine In-Flow Environment," AIAA Paper 2004-1004, 2004.
[20] Karhunen, K., "Zur Spektraltheorie Stochastischer Prozesse," *Annales Academiae Scientiarum Fennicae, Series A*, Vol. 34, 1946, pp. 3–7.
[21] Loeve, M., "Fonctions Aléatoires de Second Ordre," *Comptes rendus de l'Académie des sciences*, Vol. 220, 1945, p. 469.
[22] Hong, M., Bhatia, K., SenGupta, G., T., K., Kuruvila, G., Silva, W., Bartels, R., and Biedron, R., "Simulations of a Twin-Engine Transport Flutter Model in the Transonic Dynamics Tunnel," *International Forum on Aeroelastic and Structural Dynamics*, International Forum on Aeroelastic and Structural Dynamics Paper 2003-US-44, 2003.
[23] Lieu, T., Farhat, C., and Lesoinne, M., "POD-based Aeroelastic Analysis of a Complete F-16 Configuration: ROM Adaptation and Demonstration," AIAA Paper 2005-2295, 2005.
[24] Lieu, T., and Farhat, C., "Adaptation of POD-based Aeroelastic ROMs for Varying Mach Number and Angle of Attack: Application to a Complete F-16 Configuration," AIAA Paper 2005-7666, 2005.
[25] Lieu, T., Farhat, C., and Lesoinne, M., "Reduced-Order Fluid/Structure Modeling of a Complete Aircraft Configuration," *Computer Methods in Applied Mechanics and Engineering*, Vol. 195, Nos. 41–43, 2006, pp. 5730–5742.
doi:10.1016/j.cma.2005.08.026
[26] Lieu, T., and Farhat, C., "Adaptation of Aeroelastic Reduced-Order Models and Application to an F-16 Configuration," *AIAA Journal*, Vol. 45, No. 6, 2007, pp. 1244–1257.
doi:10.2514/1.24512
[27] Amsallem, D., Farhat, C., and Lieu, T., "Aeroelastic Analysis of F-16 and F-18/A Configurations Using Adapted CFD-Based Reduced-Order Models," *48th Structures, Structural Dynamics, and Materials Conference*, AIAA Paper 2007-2364, 2007.
[28] Amsallem, D., Farhat, C., and Lieu, T., "High-Order Interpolation of Reduced-Order Models for Near Real-Time Aeroelastic Prediction," *International Forum on Aeroelasticity and Structural Dynamics*, KTH Univ., Stockholm, Paper IF-081, 2007.
[29] Taylor, J., *Dynamics of Large Scale Structures in Turbulent Shear Layers*, Ph.D. Thesis, Clarkson Univ., New York, 2001.
[30] Taylor, J., and Glauser, M., "Towards Practical Flow Sensing and Control via POD and LSE Based Low-Dimensional Tools," *2002 ASME Fluids Engineering Division Summer Meeting*, American Society of Mechanical Engineers, Fairfield, NJ, 2002, pp. 1–9.
[31] Schmidt, R., and Glauser, M., "Improvements in Low Dimensional Tools for Flow-Structure Interaction Problems: Using Global POD," AIAA Paper 2004-0889, 2004.
[32] Lieu, T., "Adaptation of Reduced Order Models for Applications in Aeroelasticity," Ph.D. Thesis, University of Colorado, Boulder, CO, 2004.
[33] Absil, P.-A., Mahony, R., and Sepulchre, R., "Riemann Geometry of Grassmann Manifolds with a View on Algorithmic Computation," *Acta Applicandae Mathematicae*, Vol. 80, No. 2, 2004, pp. 199–220.
doi:10.1023/B:ACAP.0000013855.14971.91
[34] Boothby, W. M., *Introduction to Differentiable Manifolds and Riemanniann Geometry*, Academic Press, New York, 2003.
[35] Helgason, S., *Differential Geometry, Lie Groups and Symmetric Spaces*, American Mathematical Society, Providence, RI, 2001.
[36] Rahman, I., Drori, I., Stodden, V., Donoho, D., and Schröder, P., "Multiscale Representations for Manifold-Valued Data," *Multiscale Modeling & Simulation*, Vol. 4, No. 4, 2005, pp. 1201–1232.
doi:10.1137/050622729
[37] Edelman, E., and Arias, T. A., and Smith, S. T., "The Geometry of Algorithm with Orthogonality Constraints," *SIAM Journal on Matrix Analysis and Applications*, Vol. 20, No. 2, 1998, pp. 303–353.
doi:10.1137/S0895479895290954
[38] Chern, S. S., Chen, W. H., and Lam, K. S., *Lectures on Differential Geometry*, World Scientific, Singapore, 2000.
[39] Begelfor, E., and Werman, M., "Affine Invariance Revisited," *Proceedings of the 2006 IEEE Computer Society Conference on Computer Vision and Pattern Recognition*, Vol. 2, Inst. of Electrical and Electronics Engineers, New York, 2006, pp. 2087–2094.
[40] Wald, R. M., *General Relativity*, Univ. of Chicago Press, Chicago, 1984.
[41] Perdigao Do Carmo, M., *Riemanniann Geometry*, Birkhäuser, Boston, 1992.
[42] Späth, H., *Two Dimensional Spline Interpolation Algorithms*, A K Peters, Wellesley, MA, 1995.
[43] De Boor, C., and Ron, A., "Computational Aspects of Polynomial Interpolation In Several Variables," *Mathematics of Computation*, Vol. 58, No. 198, April 1992, pp. 705–727.
doi:10.2307/2153210
[44] Amsallem, D., and Cortial, J., *Grassmann Manifold and the Subspace Angle Interpolation Methods FRG Internal Document*, Stanford Univ., Stanford, CA, 2007.
[45] Holmes, P., Lumley, J., and Berkooz, G., *Turbulence, Coherent Structures, Dynamical Systems and Symmetry*, Cambridge Univ. Press, Cambridge, England, U.K., 1996.
[46] Geuzaine, P., Brown, G., Harris, C., and Farhat, C., "Aeroelastic Dynamic Analysis of a Full F-16 Configuration for Various Flight Conditions," *AIAA Journal*, Vol. 41, No. 3, 2003, pp. 363–371.
[47] Farhat, C., Geuzaine, P., and Brown, G., "Application of a Three-Field Nonlinear Fluid-Structure Formulation to the Prediction of the Aeroelastic Parameters of an F-16 Fighter," *Computers and Fluids*, Vol. 32, No. 1, 2003, pp. 3–29.
doi:10.1016/S0045-7930(01)00104-9
[48] Lesoinne, M., Sarkis, M., Hetmaniuk, U., and Farhat, C., "Linearized Method for the Frequency Analysis of Three-Dimensional Fluid/Structure Interaction Problems in All Flow Regimes," *Computer Methods in Applied Mechanics and Engineering*, Vol. 190, Nos. 24–25, 2001, pp. 3121–3146.
doi:10.1016/S0045-7825(00)00385-6

J. Samareh
Associate Editor